Regulation of neuroregeneration by long noncoding RNAs

Rotem Ben-Tov Perry#, **Hadas Hezroni**, **Micah Jonathan Goldrich**, and **Igor Ulitsky***
Department of Biological Regulation, Weizmann Institute of Science, Rehovot, Israel 76100

Summary

In mammals, neurons in the peripheral nervous system (PNS) have regenerative capacity following injury, but it is generally absent in the central nervous system (CNS). This difference is attributed, at least in part, to the intrinsic ability of PNS neurons to activate a unique regenerative transcriptional program following injury. Here we profiled gene expression following sciatic nerve crush in mice, and identified long noncoding RNAs (lncRNAs) that act in the regenerating neurons, and which are typically not expressed in other contexts. We show that two of these lncRNAs regulate the extent of neuronal outgrowth. We then focus on one of these, *Silc1*, and show that it regulates neuroregeneration in cultured cells and in vivo, through cis-acting activation of the transcription factor *Sox11*.

Introduction

The ability of PNS neurons to re-establish functional connections following injury depends on regulatory networks that orchestrate the regeneration program. The protein-coding components of the transcriptional response to injury are relatively well understood (Abe and Cavalli, 2008), and include induction of regeneration-associated genes (RAGs) such as the transcription factors *Jun*, *Atf3*, and *Sox11* (Jankowski et al., 2006; Raivich et al., 2004; Seijffers et al., 2007; Tsujino et al., 2000). These transcription factors direct production of mRNAs encoding adhesion molecules, cytoskeletal elements, growth factors, cytokines, neuropeptides, and other molecules involved in regeneration (Patodia and Raivich, 2012).

Advances in transcriptome mapping in the past decade revealed pervasive transcription outside of the boundaries of protein-coding genes (Guttman et al., 2009; Kapranov et al., 2007; Ravasi et al., 2006). Tens of thousands of distinct loci in the mammalian genome are transcribed into long RNA molecules, collectively called long noncoding RNAs (lncRNAs), but the functions of the vast majority of these genes remain unknown. lncRNAs are typically expressed at relatively low levels, are more tissue-specific than mRNAs, and are generally poorly conserved in evolution (Ulitsky, 2016). Perturbations of an increasing number of lncRNAs have been shown to be consequential in cultured cells, but only few functions have

---

been characterized in vivo (Perry and Ulitsky, 2016; Sauvageau et al., 2013). Genetic manipulations of some lncRNA loci affect mouse physiology during embryonic development or in adults, in particular in the nervous system (Briggs et al., 2015), but how those RNAs act is typically unknown.

Transcriptome-wide changes following PNS injury were characterized in mouse and rat using microarrays and, more recently, RNA-seq (Bosse et al., 2006; Costigan et al., 2002; Hu et al., 2016; Kubo et al., 2002; Küry et al., 2004; Lisi et al., 2017; Michaelevski et al., 2010). The activity and functions of microRNAs following PNS injuries have been extensively studied, but much less is known about the functions of lncRNAs in regeneration. Two studies reported changes in lncRNA expression in the dorsal root ganglia (DRG) following sciatic injury in rats (Yao et al., 2015; Yu et al., 2013), but the functions of those lncRNAs *in vivo*, their regulatory targets, and the extent of their conservation remain unknown. Understanding the regulatory program of the transcriptional response to injury, and how lncRNAs contribute to the intrinsic ability of PNS neurons to regenerate, is crucial for improving regenerative outcomes in both the PNS and the CNS.

Results

Identification of long noncoding RNAs expressed following sciatic nerve injury

In order to characterize lncRNAs that potentially act during neuronal regeneration in mouse, we used strand-specific RNA-seq to characterize gene expression patterns in the DRG of naive, sham-operated, and injured limbs, at three time points representing different stages of injury response and regeneration (days 1, 4, and 7 post injury, Figure 1A), and used these data to assemble a DRG transcriptome (Data S1). Unsupervised clustering of the data (see Methods) revealed various gene expression responses (Figure S1A and Data S2). Annotation of the genes in each cluster using Enrichr (Chen et al., 2013) associated different clusters with biological processes and cell types in which they are likely to be active (Figure S1A). Different clusters also overlap to varying degrees with genes differentially expressed following induction of neuronal activity (taken from (Benito et al., 2011), Figure S1B and Discussion). We focused on cluster #4, which included 1,130 genes that gradually responded to injury with peak induction at day 7, which corresponds to the active regeneration stage (Araki and Milbrandt, 2000; Kubo et al., 2002), and where genes showed large differences between injury and sham conditions (Figure 1B). The 947 protein-coding genes in this cluster included known RAGs such as *Atf3*, *Sox11*, *Sprr1a*, *Gap43*, and others, and were enriched for Gene Ontology terms relevant to regeneration (Figure S1C and Data S2). The 183 non-coding genes in the cluster included 72 genes annotated in GENCODE vM10 and 111 previously uncharacterized genes, and we annotated 66 of the 183 as bona fide distinct lncRNAs using PLAR (Hezroni et al., 2015) (Data S2). Strikingly, whereas most protein-coding genes in cluster #4 were expressed in the majority of mouse tissues, lncRNAs were highly tissue-specific, much more so than lncRNAs in the other clusters (P<10^{-10}, Figure 1C), with some injury-induced lncRNAs not expressed in any of >60 tissues profiled by the ENCODE project. Nine of the lncRNAs in cluster #4 were conserved in sequence and synteny in human (see Methods), and to the best of our knowledge none of these have undergone any functional characterization in human or mouse. For 13 of the 66 lncRNAs in

cluster #4, the closest protein-coding gene was also found in cluster #4 (mean distance from the lncRNA ~38 kb), indicating that they are co-regulated with or potentially regulate one of their neighboring genes. In contrast, for 25/66 lncRNAs, no neighboring genes within 1 Mb were found in cluster #4, suggesting independent induction following injury. We then combined these criteria with expression patterns and manual inspection and chose to focus on three lncRNAs: *Gm9866* (which we named *Sciatic Injury induced LnCRNA 1*, or *Silc1*), *1700042G15Rik* (which we named *NOncoding RNA Regulator of Injury of Sciatic nerve 1*, or *Norris1*, Figure S1D), and *5930412G12Rik* (which we named *Fzd10as1*, Figure S1E). These lncRNAs were annotated by both GENCODE and PLAR as lncRNAs, were significantly (P<0.05) up-regulated in injured neurons compared to sham operated ones at day 7, were expressed at FPKM>1 following injury, and showed evidence of sequence conservation in rat and human. We validated the up-regulation of *Sox11*, *Atf3*, and the three lncRNAs by qRT-PCR (Figure 1D-E and Figure S1F). Each of the selected lncRNAs resides in a different genomic context: *Silc1* is found in a gene desert downstream of *Sox11* (see below); *Norris1* resides in an intergenic region between *Ptpn3* and *Palm2*, two genes that do not appear to be related to neuroregeneration and are separated from *Norris1* by >50 kb; and *Fzd10as1* is transcribed divergently from a shared promoter with *Fzd10*, a Wnt receptor (Figure S1E).

Silc1 and Norris1 are required for regeneration following replating of DRG neurons

In order to study the functions of the three lncRNA candidates in neurite outgrowth after injury, we used SMARTpool siRNAs to reduce their expression in cultured DRG neurons. 48 hr after siRNA treatment the cells were re-plated in fresh medium for an additional 24 hr to mimic the injury response and to monitor axonal regrowth (Frey et al., 2015). For *Silc1* and *Norris1* we obtained >60% knockdown (KD) efficiency (Figure 2A), whereas *Fzf10as1* could not be efficiently targeted with either siRNAs or shRNAs. Reduction in *Silc1* and *Norris1* levels led to a reduction in total axonal outgrowth without any apparent effect on cell viability (Figure 2B and S2A). *Silc1* and *Norris1* therefore appear to be required for proper neurite growth in an *in-vitro* setting that simulates a PNS injury.

In order to characterize the transcriptional response following lncRNA KD, we performed RNA-seq at 72 hr following transfection of siRNAs targeting *Silc1*, *Norris1*, *Sox11*, and *Atf3*. All perturbations affected gene expression, and the responses to KD of *Silc1* and *Sox11* were strikingly similar (Spearman's r=0.37, P<10^{-15}, Figure 2C). *Silc1* KD led to a reduction in mRNA levels of *Sox11* and its downstream target *Atf3* (Jankowski et al., 2009), which we confirmed by qRT-PCR (Figure 2D and S2A). As this analysis suggested a potential mechanism for the mode of action of *Silc1*, we focused on this lncRNA for the rest of the study.

Silc1 resides ~200 kb downstream of *Sox11*, a known regulator of neurogenesis and neuronal regeneration (Jankowski et al., 2006, 2009, 2018; Jing et al., 2012) (Figure 2E and S2B). The ~600 kb region downstream of *Sox11* does not contain any protein-coding genes, and harbors a large number of putative enhancers. One of these is located in an intron of *Silc1*, decorated with histone marks associated with enhancer activity in the embryonic brain, and bound by SOX2 and SOX3, but not SOX11, in neuronal progenitors (Bergsland et

al., 2011) (Figure 2E and S2B). This region does not exhibit chromatin marks associated with active enhancers in adult tissues (Figure 2E and below). Hi-C chromosome conformation data from mouse brain (Deng et al., 2015) show that the *Silc1* locus is in spatial proximity to *Sox11*, suggesting a possible regulatory relationship between the two loci in the nervous system (Figure 2F).

Both *Silc1* and *Sox11* are expressed in various neuronal tissues (Figure S2C). In the DRG and in other neuronal contexts, *Silc1* levels are higher postnatally than in embryos, in contrast to *Sox11*, which is expressed at higher levels in embryonic tissues and is reduced after birth (Figure S2C-D). Consistent with this expression pattern, H3K4me3 chromatin mark is observed on the *Silc1* promoter in the adult cortex (Figure 2E), forebrain, and retina (see below), but not in the embryonic brain. When comparing publically available RNA-seq datasets from various neuronal injuries, including those of the CNS and PNS, *Silc1* induction was reproducible and specific to sciatic crush injury (Figure S2E-H). In bulk RNA-seq and CAGE comparisons of cell types from the cortex (Figure S2C and S2I), as well as single-cell RNA-seq data from the DRG (Figure S2J–K), *Silc1* is expressed only in neuronal cells, whereas *Sox11* is also expressed in glial cells. In the naive DRG, *Silc1* is expressed in several neuronal subtypes, predominantly in myelinated neurons, and is more subtype-specific than than *Sox11* (Figure S2J–K). We conclude that *Silc1* and *Sox11* are co-expressed in some postnatal neuronal cells, and that the combined induction of the two genes is a specific feature of regenerating peripheral neurons in the DRG.

Silc1 is a bona fide noncoding RNA based on negative PhyloCSF (Lin et al., 2011) scores throughout the locus (Figure S2B), the three coding potential predictors implemented in PLAR (Hezroni et al., 2015), and CPAT (Wang et al., 2013). There are three annotated splicing isoforms for *Silc1* in RefSeq that share the same promoter (supported by CAGE data from the FANTOM5 project, Figure 2E) and poly(A) site (supported by PolyA-seq data, Figure 2E). RT-PCR followed by sequencing showed that the two-exon ~1.4 kb isoform of *Silc1* is predominantly expressed in adult mouse brain and DRG (Figure S2L). Single molecule FISH in cultured DRG neurons and in brain cortex showed predominantly nuclear localization of *Silc1* RNA (Figure 2G and Figure S2M).

Silc1 knockdown affects regeneration through reduction in *Sox11* levels

Silc1 knockdown using siRNAs in cultured primary DRG neurons resulted in reduced mRNA and protein levels of *Sox11* and *Growth associated protein 43* (*Gap43*), which is associated with an effective regenerative response in the nervous system (Chong et al., 1994; Skene et al., 1986) (Figure 3A-B). Previous work demonstrated that cells transfected with siRNAs targeting *Sox11* exhibit a significant decrease in regeneration, as indicated by reduced neurite length and branching index (Jankowski et al., 2006). We hypothesized that the neuron growth phenotype observed following *Silc1* KD is mediated by reduction of *Sox11* levels, and attempted to rescue the KD cells with exogenous expression of *Sox11*. Infection of cultured DRG neurons with a Sox11-GFP lentivirus restored the neurite outgrowth of cells transfected with siRNAs against *Silc1* and *Sox11* to the levels observed with a control siRNA, whereas a GFP-only lentivirus had no effect (Figure 3C). We conclude that *Silc1* affects neuronal regeneration through induction of *Sox11*. To further

corroborate this model, we used the CRISPR activation (CRISPRa) system (Gilbert et al., 2013), based on dCas9-VP64, a catalytically inactive Cas9 fused to an transcriptional activator, and guide RNAs (gRNAs) targeting the *Silc1* promoter. Transfection of dCas9-VP64 and the gRNAs into two cell lines (Neuro2a/N2a and B16) that do not express *Silc1* increased expression of *Silc1* expression level by 6–8-fold in both cell lines, and increased *Sox11* expression in N2a neuronal cells, whereas no change in *Sox11* levels was observed in B16 melanoma cells (Figure S3A-B). Lentiviral injection of cultured DRG neurons with dCas9-VP64 and the gRNAs enhanced neurite outgrowth (Figure 3D, RNA levels could not be measured in infected neurons due to difficulties of recovering only the subset of cells that were infected). In order to rule out a direct effect of dCas9-VP64 on the *Sox11* promoter, which can be found in spatial proximity to *Silc1* promoter in neuronal cells (Figure 2F), we transfected N2a cells with dCas9-VP64 and five different gRNAs targeted directly to the *Sox11* promoter, and observed no effect on either *Silc1* or *Sox11* levels (Figure S3D). In contrast to the effects of *Silc1* CRISPRa, transfection of N2a cells with an expression plasmid encoding *Silc1* cDNA increased *Silc1* levels by >5,000-fold, but had no effect on *Sox11* levels (Figure S3C). Taken together, specifically in neuronal cells, increase of *Silc1* transcription leads to up-regulation of *Sox11* mRNA levels in *cis* and increased neurite outgrowth.

Silc1 knockout mice have reduced *Sox11* levels in neuronal cells and exhibit delayed regeneration following injury

In order to examine *Silc1* function *in vivo*, we generated *Silc1* knockout (KO) mice using CRISPR/Cas9 with gRNAs flanking the *Silc1* promoter and exon 1 (Figure 4A and S4A). These mice were born at expected Mendelian ratios (Figure S4B) and exhibited no gross morphological defects (Figure S4C). *Silc1* promoter KO resulted in >90% decrease in *Silc1* levels in cultured adult DRG neurons, DRG tissue samples, and in adult brain, as measured by qRT-PCR and RNA-seq (Figure 4B-C). *Sox11* levels in the DRG tissue samples did not change significantly at three tested embryonic or postnatal (Figure 4D), and a significant reduction was observed in the brain only in the adult (eight weeks old mice). In adult cultured DRG neurons following replating, *Silc1*^{-/-} mice exhibited a ~60% decrease in *Sox11* mRNA levels (Figure 4B), and decrease in SOX11 protein as detected by staining (Figure 4E) and Western blot (WB) of adult brain extracts (Figure 4F; SOX11 could not be detected by WB of DRG extract from either WT or *Silc1*^{-/-} mice). Therefore, *Silc1* appears to regulate *Sox11* levels only in adult neurons, and not during embryonic or early postnatal development, where *Sox11* is presumably primarily regulated by other elements.

In order to test if loss of *Silc1* affected expression from the *cis* allele of *Sox11*, we crossed a *Silc1*^{+/-} C57BL/6J mouse with WT FVB/NJ mice to obtain *Silc1*^{+/-} heterozygotes in which the *Silc1+* allele was found in *cis* to a G allele of the rs4222054 SNP in the *Sox11* 3' UTR, and the *Silc1-* allele in *cis* to an A allele. We then used allele-specific RT-PCR to compare the expression of *Sox11* in replated cultured DRG neurons from *Silc*^{+/+} and *Silc*^{+/-} mixed background mice, and found that loss of *Silc1* led to reduction in *Sox11* expression only from the allele in cis to deletion (Figure 4H and S4D), supporting a model where *Silc1* is acting to increase *Sox11* transcription from the allele that is found on the same chromosome and in spatial proximity to the *Silc1* locus (Figure 2F).

In cultured DRG, *Silc1* KO led to a reduction in total axonal outgrowth following replating (Figure 4G), recapitulating the phenotype observed upon *Silc1* RNA depletion with siRNAs (Figure 2B).To determine whether loss of *Silc1* expression and the reduction in *Sox11* levels have functional effects on nerve regeneration and recovery, we examined recovery from sciatic nerve crush in WT and *Silc1*^{-/-} mice following sciatic nerve injury using CatWalk gait analysis (Bozkurt et al., 2008; Kappos et al., 2017; Perry et al., 2012). In this system, animals are followed by video recording while crossing a glass runway, enabling examination of gait and locomotion and subsequent analyses of both dynamic and static gait parameters. This system allows testing the outcome of the injury and the functional recovery in a comprehensive manner. Following unilateral sciatic nerve crush in the right hind leg, mice were monitored over a period of 23 days at 2–4 day intervals. Before sciatic injury, no significant differences were observed in basal gait parameters between WT and *Silc1*^{-/-} mice. One day after injury, significant reduction in both static and dynamic gait parameters was observed for the injured limb in both genotypes. The injured mice exhibited reductions in print area (the area of the paw that touches the surface when stepping) and swing speed (a parameter combining stride length and swing duration) for the injured limb (Figure 5A). Recovery, manifested by improvement in both these parameters over time, was evident in both genotypes but at significantly different rates (Figure 5A). The differences between the genotypes were most prominent at five days post injury, when the WT animals were already making appreciable use of the injured limb while the *Silc1*^{-/-} mice were not (significantly lower print area in *Silc1*^{-/-} vs WT animals, P<0.005, Figure 5A). Furthermore, WT mice reached an asymptote in their recovery process on day 5, whereas *Silc1*^{-/-} mice reached an asymptote only on day 11. These observations show that loss of *Silc1* results in functional consequences in the recovery process.

To support the behavioral data, we examined axonal morphologies in sciatic nerve using GAP43 staining at day 1, 4, 7, and 25 following sciatic injury. GAP43 is expressed at elevated levels in differentiating neurons during development and regeneration, and is commonly used as a marker of regeneration in the adult nervous system (Van der Zee et al., 1989). Significant differences were seen in branch length between WT and *Silc1*^{-/-} mice at 2 and 3 mm proximal to the injury site four and seven days post injury, indicating reduced regeneration in axons of neurons lacking *Silc1* (Figure 5B-C and Figure S5). Thus, behavioral and histological parameters show delayed regeneration of sensory neurons in *Silc1*^{-/-} mice.

Loss of *Silc1* results in dysregulated gene expression in the DRG following injury

In order to better understand the consequences of *Silc1* deficiency, we used RNA-seq to characterize gene expression in the whole adult brain and in the DRG of *Silc1*^{-/-} mice and their WT littermates. DRG were profiled in naive conditions as well as 4 and 7 days following injury or sham operation. Few changes were present in the naive DRG and in the brain, suggesting limited effects of loss of *Silc1* expression during development. In contrast, substantial changes were observed at four days following injury, with some similarity in changes in injured and in sham-operated mice (Figure 6A-B and Data S3), which may stem from the induction of *Silc1* and *Sox11* following the sham operation (Figure 1D-E). Beyond these differences, and consistently with the phenotype of delayed but nevertheless full

regeneration, the overall gene expression changes between the injured and the sham operated DRG were similar in the WT and *Silc1*⁻/⁻ mice, in particular at day 7 (Figure S6). When examining changes in genes belonging to particular clusters of expression patterns following injury (Figure S1A), injured DRG from *Silc1*⁻/⁻ mice displayed significantly reduced expression of genes normally up-regulated following injury (clusters #4 and #6, Figure 6B), with a particularly prominent reduction at day 4 in expression of genes in cluster #6, which included genes induced by day 4 after injury (Figure S1A). Further, there was increased expression in *Silc1*⁻/⁻ DRG of genes that are typically repressed following injury (clusters #10 and #14, Figure S1A and Figure 6B). These changes were also stronger at day 4, consistent with the more prominent peak difference in behavioral parameters at the earlier time point. Genes in injury-related clusters exhibited no substantial changes in expression in the naive DRG (Figure 6B). Consistent with the changes in gene expression following injury, we also observed a significant reduction in SOX11 protein levels at day 4 following injury (Figure 6C).

In order to characterize changes in chromatin accessibility, we performed ATAC-seq (Buenrostro et al., 2013) on 4 days injured or sham-operated DRG from WT and *Silc1*⁻/⁻ mice. When considering 71,615 regions found to be accessible in one of the conditions or 15,468 peaks overlapping promoters of our DRG transcriptome (see Methods), regions overlapping binding peaks of *Sox11* in neurons (from (Bergsland et al., 2011)) exhibited reduced accessibility following injury compared to other peaks, and compared to sham operated DRG (Figure 6D). These differences suggest that loss of *Silc1* leads to a significant perturbation in the regulation of promoter and enhancer regions bound by *Sox11*.

Discussion

Using RNA-seq we characterized the changes in gene expression in the mouse DRG following sciatic nerve injury and grouped the genes into 17 clusters. Several of these clusters showed consistent responses to injury, of which we focused on lncRNAs in cluster #4, which were gradually induced following injury, peaking at day 7. Another interesting cluster is #13, which represents an early injury-specific response that peaks at day 1. Several recent studies (reviewed in (Mahar and Cavalli, 2018)) showed that some genes acting early following regeneration are also involved in neuronal activity. Indeed, we find an overlap between cluster #13 and neuronal activity-driven gene expression profiles. Cluster #13 contains 12 lncRNAs, which may also have such a dual function.

lncRNAs are typically poorly conserved in evolution, though over a thousand are conserved throughout mammals and around one hundred lncRNAs are retained across vertebrates (Hezroni et al., 2015; Ulitsky, 2016; Ulitsky et al., 2011). *Silc1* is conserved in sequence and expression in various eutherian mammals, where it is robustly expressed in neuronal tissues (Figure 7A). There are four prominent regions of high sequence conservation in this locus (annotated cr1–4 in Figure 7A). Only cr1, which corresponds to the first exon of *Silc1*, is part of the exonic sequence of *Silc1* throughout eutherian mammals (the five species in Figure 7A, as well as rhesus and marmoset (Hezroni et al., 2015)), and cr2 and cr3 overlap introns or exons of *Silc1* in all species. Region cr2 corresponds to a region showing extensive enhancer marks in the mouse embryo, which is bound by Sox2 and Sox3 in

neuronal progenitors (Figure 2E), but does not appear to be active in the adult DRG, regardless of injury (see below). Both cr2 and cr3 are conserved in opossum, chicken, and lizard, and cr3 is conserved in *Xenopus*. However, in those additional species, there is no evidence for lncRNA transcription in the vicinity of cr2–3 in any of several profiled tissues, which include whole adult brain (Hezroni et al., 2015). This suggests that *Silc1* appeared and gained a regulatory function in mammals within a genomic region that previously had a lncRNA-independent function, most likely as an embryonic enhancer of *Sox11*.

The fourth conserved region in the *Silc1* locus, cr4, lies outside of the *Silc1* transcription unit in mouse (Figure 7A), and corresponds to a promoter of a different lncRNA, *LOC400940*, in human. *LOC400940* is more broadly expressed than *SILC1* in human cell lines, and plausibly evolved from an enhancer RNA that gained transcription in the primate lineage, as there is evidence for a transcript starting at cr4 also in rhesus, but not in other mammals. *Silc1* conservation pattern thus places it in a broad group of "class 2" lncRNAs, which have a single conserved exonic sequence (in exon 1) nested in a longer transcript that exhibits a rapidly evolving exon-intron architecture (Ulitsky, 2016). Functional sequences or structures in *Silc1* RNA, if any, are thus likely to be present in the first exon.

We show here that *Silc1* facilitates up-regulation of *Sox11* in the injured DRG and is required for maintaining *Sox11* expression levels in the adult brain. Genomic data from various systems suggest that this regulation occurs primarily after birth. In the DRG, *Silc1* levels are much higher postnatally than in the embryo, in contrast to *Sox11*, which is more highly expressed in the embryo (Figure S2C-D). Similar dynamics are observed in other neuronal systems that were profiled at higher resolution, including the retina (Aldiri et al., 2017) and the forebrain (ENCODE project) (Figure S7A). In those systems, *Sox11* levels peak around E14.5, whereas *Silc1* expression is observed primarily postnatally. These expression patterns correlate with chromatin marks in the region: the levels of the promoter mark H3K4me3 at the *Silc1* promoter increase postnatally, and correlate with *Silc1* expression levels. The levels of H3K27ac, a mark of active enhancers, are high at the cr2 region in *Silc1* intron in the embryo, and are then reduced to background levels postnatally. Together with our results showing that up-regulation of *Silc1* facilitates *Sox11* expression in adult neuronal cells, these data suggest a switch in *Sox11* regulation by the *Silc1* locus that occurs around birth, where loss of activity of the enhancer in *Silc1* intron coincides with gain of *Silc1* expression. Importantly, it is possible that the phenotypic effects we observed in *Silc1*^{-/-} mice are due to loss of *Silc1* activity in late embryonic or postnatal development, and not due to its functions following the injury. The lack of appreciable difference between WT and *Silc1*^{-/-} mice in basal gait parameters and the limited differential expression in naive DRG or adult brain (Figure 6A) argue against this possibility, but a conclusive analysis will require establishment of a conditional KO mouse for *Silc1*, and the activation of the KO specifically in the DRG sensory neurons in the adult mice, prior to injury. We also note that regeneration occurs, albeit at a slower rate, in the *Silc1*^{-/-} mice, and *Sox11* is induced at day 7 following injury to similar levels in WT and *Silc1*^{-/-} mice, and so compensatory mechanisms likely exist for *Sox11* induction. These presumably involve other enhancers in the ~2Mb gene desert surrounding *Sox11*, and may overlap with the mechanisms activating *Sox11* in embryonic and/or glial cells, where *Silc1* is not expressed at appreciable levels.

The mechanism through which *Silc1* activates *Sox11* expression is currently unknown. *Silc1* activity resembles that of *Upperhand* and *ThymoD* lncRNAs (Anderson et al., 2016; Isoda et al., 2017), whose transcription is required for the activation of their proximal genes *Hand2* and *Bcl11b*, respectively, during development, also through a largely unknown mechanism. However, unlike *Upperhand*, where reduction of the RNA levels did not appear consequential for *Hand2* levels, the RNA product of *Silc1* appears to be required for its function, as we observed similar effects following promoter deletion, which abolishes transcription, and when using siRNAs that degrade the RNA product of *Silc1*. It was suggested that Upperhand functions through modulation of activity of enhancers overlapping its transcription unit (Anderson et al., 2016). *Silc1* transcription unit overlaps regions that bear enhancer-associated chromatin marks in the embryo, but those do not appear accessible in our ATAC-seq data, which does show an increase in accessibility of the *Silc1* promoter following injury (Figure S7B). Our sensitivity to detect differential accessibility of regions in the *Silc1* locus might be limited by the complexity of the DRG tissue, although we are able to detect differential accessibility in other regions (Figure S7B). *Silc1* activity and induction of *Sox11* following injury are thus likely unrelated to those enhancer regions. It is possible that *Silc1* activation, or the deletion of the *Silc1* promoter, affect the spatial contact landscape in the gene desert flanking *Sox11*, akin to some lncRNAs like *CCAT1* (Xiang et al., 2014). Hi-C analysis of neuronal differentiation data (Bonev et al., 2017), suggest that contacts between *Sox11* and the broad region surrounding *Silc1* are readily detectable in neuronal progenitors, where *Silc1* levels are very low (~100 times lower than in the DRG following injury, Figure S7C-D), and so we think that it is unlikely that *Silc1* expression is important for the establishment or maintenance of spatial contacts between *Silc1* and *Sox11* loci. Another possibility is that *Silc1* affects release of a paused RNA polymerase at the *Sox11* promoter, as has been reported for some enhancer RNAs (eRNAs) and lncRNAs (Ntini et al., 2018; Schaukowitch et al., 2014). This possible mode of action is consistent with the observation that there is no evident change in chromatin accessibility at the *Sox11* promoter following injury (Figure S7B), and with the substantial Pol2 pausing at the *Sox11* promoter in neuronal tissues (Figure S7E). Exploring these options is currently hindered by the limited material for chromatin-associated applications in the DRG, and by the fact that we could not identify any mouse cell line that expresses *Silc1*.

Interestingly, lncRNAs are overall enriched in regions flanking genes encoding transcriptional regulators (Guttman et al., 2009; Ulitsky et al., 2011) and other functional lncRNAs have recently been observed downstream of other SOX genes. *ROCR/ LOC102723505* is found in a gene desert downstream of *Sox9*, and was shown to be required for induction of *Sox9* during chondrogenic differentiation of mesenchymal stem cells (Barter et al., 2017). *CASC15* in human and *2610307P16Rik/Casc15* in mouse are lncRNAs found ~70 kb downstream of *Sox4*, and KD or KO of these lncRNAs resulted in reduction of *Sox4* levels in both species (Fernando et al., 2017). *Peril* is a lncRNA essential for viability in mice (Sauvageau et al., 2013), which is found ~110 kb downstream of *Sox2*. *Peril* expression domain in the mouse brain overlaps that of *Sox2* (Goff et al., 2015). *Sox1* and *Sox2* also have overlapping lncRNA transcripts that span hundreds of kb, containing the SOX gene in one of their introns (Ahmad et al., 2017; Amaral et al., 2009). While there is currently neither an obvious common origin nor evident commonalities in the mechanisms

of action of those lncRNAs, the similarity in their activities and genomic context suggest that *cis*-acting regulation by lncRNAs is a common and potentially ancient theme in the biology of the SOX gene family.

Norris1, whose induction following injury we also identified here as required for proper regeneration in cultured DRG, is an example of an exquisitely tissue-specific lncRNA. *Norris1* is highly expressed in the testis (Figure S1D), but we did not observe substantial expression of *Norris1* in any tissues, cell lines, or treatments measured by the ENCODE or FANTOM5 projects, or other datasets assembled in the EBI expression atlas. Interestingly, in the testis, *Norris1* serves as a precursor for a large number of piRNAs (Figure S1D). We therefore profiled small RNAs in naive and injured DRG, but did not observe any evidence for small RNAs emanating from this locus (Data S4), suggesting that *Norris1* does not act through the piRNA pathway in neuroregeneration. *Norris1* also does not appear to act in *cis*, as none of the adjacent genes appeared induced in regeneration, and inspection of HiC data from various mouse tissues did not suggest any genes or regions that form frequent contacts with the *Norris1* locus.

It is well appreciated that lncRNAs are expressed in a much more tissue-specific manner than protein-coding genes (Cabili et al., 2011). Indeed, we find that many of the lncRNAs that act in the DRG during neuroregeneration following injury are highly specific in their expression, much more so than the classical and well-studied protein-coding RAGs (Figure 1C). Using data from other studies, we observed that some of those are only observed in this specific physiological context; others, like *Norris1*, are expressed in few other contexts but are not found in the CNS, whereas others, like *Silc1*, act in a subset of conditions in the CNS and PNS, where they are only induced following injuries associated with neuroregeneration in the PNS (Figure S2E-H). Changes in lncRNA activity may thus explain some of the differences in the regulatory programs activated following injury in different parts of the nervous system; therefore, their manipulation using the oligonucleotide- and CRISPR-based therapeutic interventions (Nguyen and Wong, 2017) carries the potential to specifically reprogram these cells following injury and potentially improve regenerative outcomes following neuronal lesions.

STAR Methods

Contact for Reagent and Resource Sharing

Further information and requests for resources and reagents should be directed to and will be fulfilled by Igor Ulitsky (igor.ulitsky@weizmann.ac.il).

Experimental Model and Subject Details

Animals—The study was conducted in accordance with the guidelines of the Weizmann Institutional Animal Care and Use Committee (IACUC). C57black6 Ola HSD male mice were purchased from Harlan Laboratories (Rehovot, Israel). All other mouse strains were bred and maintained at the Veterinary Resources Department of the Weizmann Institute.

Sciatic nerve crush—Mice (6-8 weeks) were anesthetized with an intraperitoneal injection of xylazine and ketamine (10 mg/kg body weight). A 1-cm-long incision was made

in the skin of the thigh perpendicular to the femur. A small incision was made between the thigh muscles and the muscles were separated by insertion and opening of the tip of the scissors between the muscles. The sciatic nerve was identified and pulled out using 45° forceps. The tissue was crushed using fine forceps (Dumont no. 4) three times for 30 seconds at mid-thigh level. The sciatic was positioned back in its place by gently pulling the hind leg. The incision was closed using reflex wound clips.

DRG cultures—Adult mouse DRGs were dissociated for neuron cultures with 100 U of papain followed by 1 mg/ml collagenase-II and 1.2 mg/ml dispase. The ganglia were then triturated in HBSS, 10 mM glucose, and 5 mM HEPES (pH 7.35). Neurons were recovered through percoll, plated on laminin, and grown in F12 medium for 48 hours (Hanz et al., 2003; Perlson et al., 2005; Rishal et al., 2010).

Method Details

siRNA treatment—Adult male mice DRG cultures were transfected with siGenome siRNAs (Table S2) using DharmaFect 4 (Dharmacon), replated 24 hr later, and imaged 72 hr after transfection. Neuronal images were acquired at X10 magnification on an ImageXpress Micro (Molecular Devices) automated microscopy system and quantified using WIS-Neuromath (www.wisdom.weizmann.ac.il/~vision/NeuroMath/). The parameters reported include total outgrowth, defined as the sum of lengths of all processes and branches per cell. Statistical significance was evaluated using Student's t test.

Generation of *Silc1* KO mice—The CRISPR KO mice were generated as in (Wang et al., 2013). *Silc*1 KO mice were generated by standard procedures at the Weizmann transgenic core facility using two single guide RNAs (sgRNAs) with recognition sites before the *Silc1* promoter (chr12:27160159, mm10 assembly) and after exon 1 (chr12:27160890, mm10 assembly).

Silc1$^{-/-}$ mice were identified by genotyping and sequencing. Lines were bred and maintained on C57BL/6 background at the Veterinary Resources facility of the Weizmann Institute. All the experiments were done on 6–8 weeks old mice from F3 generation.

Lentivirus production, plasmids, and transfections—Lentivirus production was performed as previously described (Tiscornia et al., 2006). All transfections were performed using Lipofectamine 3000 reagent (Thermo Fisher Scientific) using Neuro 2a or B16 melanoma cells from mouse that were routinely cultured in DMEM containing 10% fetal bovine serum and 100 U penicillin/0.1 mg ml^{-1} streptomycin at 37 °C in a humidified incubator with 5% CO_2.

For *Silc1* overexpression, *Silc1* was cloned downstream of a CMV promoter in a pcDNA3.1(+) vector. We also introduced GFP replacing neomycin under SV40 promoter into the same vector, and as control we used pcDNA3.1(+) GFP (Invitrogen). For *Sox11* rescue experiments, *Sox11* was cloned into pLenti CMV GFP between BamHI sites. For *Silc1* induction from its endogenous locus using CRISPRa, we used pHAGE EF1alpha dCAS-vp64-HA (Addgene 50918) and pKLV-U6gRNA-BFP (Addgene 50946) vectors.

CatWalk gait analysis—Before the surgery, male mice (6-8 weeks) were trained three times for baseline value measurements (Noldus Information Technology, The Netherlands). Data were collected and analyzed with CatWalk™XT 10.6 (Noldus). Data sampling per mouse per day of assessment included five runs. Post operation data collection were performed 1, 3, 5, 7, 11, 15, 19, and 23 days following the sciatic nerve crash lesion. The collected indices included print area (represents the complete print including all frames that makes up a stance) and swing speed (computed from stride length and swing duration and is expressed in pixels/second). Data are expressed as a ratio between the ipsilateral to the contralateral hind paws divided by baseline value of each mouse. Data are expressed as mean ± standard-error-of-the-mean (SEM). A p-value of 0.05 was regarded as the threshold of statistical significance.

Western blot and immunofluorescence—Cultured DRG cells from WT and *Silc1*$^{-/-}$ mice were fixed with 4% paraformaldehyde 24 hr after re-plating and stained with anti-NFH for process length determination. Sciatic nerves were fixed with 4% paraformaldehyde for 3 hr followed by overnight in 30% sucrose with overhead rotation. Tissue was frozen in Tissue-Tek O.C.T compound (Sakura 4583) blocks and sectioned using a Leica cryostat (CM3050) at 10 micrometers thickness. Blocking/permeabilization were done with 5% donkey serum, 2% BSA, and 0.1% Triton X-100 in PBS. Primary antibodies were diluted in permeabilization buffer. Imaging was done using Leica DM4000 B microscopy with Leica DFC365 FX CCD microscope camera and Leica application suite (LAS) X software.

Western blots were carried out as previously described (Hanz et al., 2003; Perlson et al., 2005). For Westerns, the samples were resolved on 10% SDS PAGE, transferred to nitrocellulose and incubated with primary antibodies overnight. AzureSpectra fluorescent 700 anti-mouse and 800 anti-rabbit (Azure biosystem) were used as the secondary antibodies for fluorescent quantification of Western blots. Blots were imaged on an Azure Imager system.

Quantification of immunofluorescence—The immunofluorescence staining were quantified using Fiji (ImageJ) analysis software. For GAP43 staining a custom script was used to measure the branch length of new fibers in the sciatic in different distances from the injury site. New neurites were located based on GAP43 channel, tubeness was used to enhance the fibers, threshold with fixed values was used to filter out small segments. For each image, ordered by distance from the injury point, a mask of the neurites in the area was created and further processed using the GDSC Skeleton Analyzer plugin.

Single-molecule FISH and immunofluorescence—Library of 48 probes (Table S3) was designed the target the mouse *Silc1* RNA sequence (Stellaris RNA FISH probes, Biosearch Technologies). Hybridization conditions and imaging were as described previously (Lyubimova et al., 2013) except for the addition of immunofluorescence detection of chicken anti-NF-H (Abcam Ab72996). For immunofluorescence, the antibody was diluted in hybridization buffer (1:1000), added to the FISH probes and incubated overnight at 30 °C. Secondary antibody Cy2-conjugated donkey anti-chicken (1:1000) was added to glucose oxidase (GLOX) buffer for 20 min in room temperature. smFISH imaging was performed on a Nikon-Ti-E inverted fluorescence microscope with a 100 × oil-

immersion objective and a Photometrics Pixis 1024 CCD camera using MetaMorph software as previously described (Bahar Halpern and Itzkovitz, 2016).

RNAscope FISH—Brains were immediately frozen on dry ice in tissue-freezing medium. Brains were sliced on a cryostat (Leica CM 1950) into 8-μm sections, adhered to SuperFrost Plus slides (VWR), and immediately stored at −80 °C until use. Samples were processed according to the ACD RNAscope Fluorescent Multiplex Assay manual using *Silc1* probes-RNAscope 2.5vs probe ″Mm GM9866″ Cat No. 536709 (Wang et al., 2012).

RNA extraction and sequencing—Total RNA was extracted from total DRGs pooled from three male mice using the TRIREAGENT (MRC) according to the manufacturer's protocol. Strand-specific mRNA-seq libraries were prepared from 300-500 ng total RNA using the TruSeq Stranded mRNA Library Prep Kit (Illumina), according to the manufacturer's protocol, and sequenced on a NextSeq 500 machine to obtain 75 nt and 150 nt single- or paired-end reads. All RNA-seq dataset is deposited in GEO database under the accession GSE111497.

ATAC-seq—ATAC-seq was performed as previously described (Buenrostro et al., 2013) with minor adjustment for application to tissue material. Six fresh L4-L6 DRGs were extracted in 100 μl ice cold cell lysis buffer (10mM Tris-HCl pH 7.4, 10mM NaCl, 3mM $MgCl_2$, 0.5% IGEPAL CA-630) for 5 minutes on ice, then a 21g needle on a 1 mL syringe was used to shear the tissue through the needle 5 times. Libraries were sequence with paired-end sequencing on Illumina NextSeq 500.

Quantification and Statistical Analysis

Transcriptome reconstruction—For transcriptome reconstruction, reads were mapped to the mouse genome (mm10) using HiSat (Kim et al., 2015), and expression levels of GENCODE vM10 transcripts were first quantified using RSEM (Li and Dewey, 2011). Transcripts that were expressed with an FPKM 0.5 in at least one condition were used as reference for a transcriptome reconstruction using StringTie (Pertea et al., 2015), which was applied separately in each condition, and the resulting transcript models were then merged into a unified transcriptome (using the filtered GENCODE transcriptome and stringtie --merge with parameters -m 300 -c 0.5 -F 0.5 -f 0.05). The expression levels of those transcripts were then quantified using RSEM, and normalized using DESeq2. lncRNAs in the transcriptome were then identified using PLAR (Hezroni et al., 2015). We then focused on 12,816 genes that showed a difference of expression of at least 0.25 in at least one condition compared to the naive DRG, and clustered those genes using CLICK (Sharan and Shamir, 2000) as implemented in Expander (Ulitsky et al., 2010).

RNA-seq analysis and differential expression—For generation of coverage tracks, RNA-seq reads were mapped to the mouse genome using STAR (Dobin et al., 2013). Differential expression following siRNA-mediated knockdowns was performed using DESeq2 (Love et al., 2014). Public RNA-seq datasets were downloaded from SRA database and quantified using RSEM.

ATAC-seq data analysis—Three replicates were combined for all the analysis into four groups (WT/KO, injury/sham). Reads were mapped to the mouse genome (mm10 assembly) using Bowtie2 with the "-X 2000" parameter. As ATAC-seq libraries typically contain multimodal fragment length distributions, and those were slightly different for different repeats, we performed the following subsampling procedure to unify the fragment length distribution. All the reads were first binned by their inferred insert length (obtained from the BAM file). We then traversed the bins, and kept in each bin an equal number of reads from each of the four groups (matching the read number in each bin to number of reads in the group which had the least reads in the bin), subsampling reads at random. This procedure resulted in 73,944,617 paired-end read mappings per group. Peaks of accessible chromatin where then found in each group using MACS2 with the following parameters "callpeak -B -format BAMPE -g mm". The peaks from the four groups were merged using bedtools, and the heights of the merged peaks in each group were computed using bigWigAverageOverBed with -minMax parameter. Overlaps of peaks with ChIP-seq based peaks of Sox11 binding (Bergsland et al., 2011) were found using the GenomicRanges library in R. KO/WT ratios of the peak heights were normalized by the ratios of the sum of all the peaks in each comparison.

Data and Software Availability

Accession numbers—All the RNA-seq data has been deposited in the GEO database under ID code GSE111497 and ATAC-seq data under ID code GSE119489.

Supplementary Material

Refer to Web version on PubMed Central for supplementary material.

Acknowledgments

References

Abe N, Cavalli V. Nerve injury signaling. Curr Opin Neurobiol. 2008; 18:276–283. [PubMed: 18655834]

Ahmad A, Strohbuecker S, Tufarelli C, Sottile V. Expression of a SOX1 overlapping transcript in neural differentiation and cancer models. Cell Mol Life Sci. 2017; 74:4245–4258. [PubMed: 28674729]

Aldiri I, Xu B, Wang L, Chen X, Hiler D, Griffiths L, Valentine M, Shirinifard A, Thiagarajan S, Sablauer A, et al. The Dynamic Epigenetic Landscape of the Retina During Development, Reprogramming, and Tumorigenesis. Neuron. 2017; 94:550–568.e10. [PubMed: 28472656]

Amaral PP, Neyt C, Wilkins SJ, Askarian-Amiri ME, Sunkin SM, Perkins AC, Mattick JS. Complex architecture and regulated expression of the Sox2ot locus during vertebrate development. RNA. 2009; 15:2013–2027. [PubMed: 19767420]

Anderson KM, Anderson DM, McAnally JR, Shelton JM, Bassel-Duby R, Olson EN. Transcription of the non-coding RNA upperhand controls Hand2 expression and heart development. Nature. 2016; 539:433–436. [PubMed: 27783597]

Araki T, Milbrandt J. Ninjurin2, a novel homophilic adhesion molecule, is expressed in mature sensory and enteric neurons and promotes neurite outgrowth. J Neurosci. 2000; 20:187–195. [PubMed: 10627596]

Bahar Halpern K, Itzkovitz S. Single molecule approaches for quantifying transcription and degradation rates in intact mammalian tissues. Methods. 2016; 98:134–142. [PubMed: 26611432]

Barter MJ, Gomez R, Hyatt S, Cheung K, Skelton AJ, Xu Y, Clark IM, Young DA. The long non-coding RNA ROCR contributes to SOX9 expression and chondrogenic differentiation of human mesenchymal stem cells. Development. 2017; 144:4510–4521. [PubMed: 29084806]

Benito E, Valor LM, Jimenez-Minchan M, Huber W, Barco A. cAMP response element-binding protein is a primary hub of activity-driven neuronal gene expression. J Neurosci. 2011; 31:18237–18250. [PubMed: 22171029]

Bergsland M, Ramsköld D, Zaouter C, Klum S, Sandberg R, Muhr J. Sequentially acting Sox transcription factors in neural lineage development. Genes Dev. 2011; 25:2453–2464. [PubMed: 22085726]

Binder JX, Pletscher-Frankild S, Tsafou K, Stolte C, O'Donoghue SI, Schneider R, Jensen LJ. COMPARTMENTS: unification and visualization of protein subcellular localization evidence. Database. 2014; 2014

Bonev B, Mendelson Cohen N, Szabo Q, Fritsch L, Papadopoulos GL, Lubling Y, Xu X, Lv X, Hugnot J-P, Tanay A, et al. Multiscale 3D Genome Rewiring during Mouse Neural Development. Cell. 2017; 171:557–572.e24. [PubMed: 29053968]

Bosse F, Hasenpusch-Theil K, Küry P, Müller HW. Gene expression profiling reveals that peripheral nerve regeneration is a consequence of both novel injury-dependent and reactivated developmental processes. J Neurochem. 2006; 96:1441–1457. [PubMed: 16478531]

Bozkurt A, Deumens R, Scheffel J, O'Dey DM, Weis J, Joosten EA, Führmann T, Brook GA, Pallua N. CatWalk gait analysis in assessment of functional recovery after sciatic nerve injury. J Neurosci Methods. 2008; 173:91–98. [PubMed: 18577402]

Briggs JA, Wolvetang EJ, Mattick JS, Rinn JL, Barry G. Mechanisms of Long Noncoding RNAs in Mammalian Nervous System Development, Plasticity, Disease, and Evolution. Neuron. 2015; 88:861–877. [PubMed: 26637795]

Buenrostro JD, Giresi PG, Zaba LC, Chang HY, Greenleaf WJ. Transposition of native chromatin for fast and sensitive epigenomic profiling of open chromatin, DNA-binding proteins and nucleosome position. Nat Methods. 2013; 10:1213–1218. [PubMed: 24097267]

Cabili MN, Trapnell C, Goff L, Koziol M, Tazon-Vega B, Regev A, Rinn JL. Integrative annotation of human large intergenic noncoding RNAs reveals global properties and specific subclasses. Genes Dev. 2011; 25:1915–1927. [PubMed: 21890647]

Chen EY, Tan CM, Kou Y, Duan Q, Wang Z, Meirelles GV, Clark NR, Ma'ayan A. Enrichr: interactive and collaborative HTML5 gene list enrichment analysis tool. BMC Bioinformatics. 2013; 14:128. [PubMed: 23586463]

Chong MS, Reynolds ML, Irwin N, Coggeshall RE, Emson PC, Benowitz LI, Woolf CJ. GAP-43 expression in primary sensory neurons following central axotomy. J Neurosci. 1994; 14:4375–4384. [PubMed: 8027785]

Costigan M, Befort K, Karchewski L, Griffin RS, D'Urso D, Allchorne A, Sitarski J, Mannion JW, Pratt RE, Woolf CJ. Replicate high-density rat genome oligonucleotide microarrays reveal hundreds of regulated genes in the dorsal root ganglion after peripheral nerve injury. BMC Neurosci. 2002; 3:16. [PubMed: 12401135]

Deng X, Ma W, Ramani V, Hill A, Yang F, Ay F, Berletch JB, Blau CA, Shendure J, Duan Z, et al. Bipartite structure of the inactive mouse X chromosome. Genome Biol. 2015; 16:152. [PubMed: 26248554]

Dobin A, Davis CA, Schlesinger F, Drenkow J, Zaleski C, Jha S, Batut P, Chaisson M, Gingeras TR. STAR: ultrafast universal RNA-seq aligner. Bioinformatics. 2013; 29:15–21. [PubMed: 23104886]

Durand NC, Robinson JT, Shamim MS, Machol I, Mesirov JP, Lander ES. Aiden EL:Juicebox Provides a Visualization System for Hi-C Contact Maps with Unlimited Zoom. Cell Syst. 2016; 3:99–101. [PubMed: 27467250]

Eden E, Navon R, Steinfeld I, Lipson D, Yakhini Z. GOrilla: a tool for discovery and visualization of enriched GO terms in ranked gene lists. BMC Bioinformatics. 2009; 10:48. [PubMed: 19192299]

Fagerberg L, Hallstrom BM, Oksvold P, Kampf C, Djureinovic D, Odeberg J, Habuka M, Tahmasebpoor S, Danielsson A, Edlund K, et al. Analysis of the human tissue-specific expression by genome-wide integration of transcriptomics and antibody-based proteomics. Mol Cell Proteomics. 2014; 13:397–406. [PubMed: 24309898]

Fernando TR, Contreras JR, Zampini M, Rodriguez-Malave NI, Alberti MO, Anguiano J, Tran TM, Palanichamy JK, Gajeton J, Ung NM, et al. The lncRNA CASC15 regulates SOX4 expression in RUNX1-rearranged acute leukemia. Mol Cancer. 2017; 16:126. [PubMed: 28724437]

Frey E, Valakh V, Karney-Grobe S, Shi Y, Milbrandt J, DiAntonio A. An in vitro assay to study induction of the regenerative state in sensory neurons. Exp Neurol. 2015; 263:350–363. [PubMed: 25447942]

Gilbert LA, Larson MH, Morsut L, Liu Z, Brar GA, Torres SE, Stern-Ginossar N, Brandman O, Whitehead EH, Doudna JA, et al. CRISPR-mediated modular RNA-guided regulation of transcription in eukaryotes. Cell. 2013; 154:442–451. [PubMed: 23849981]

Goff LA, Groff AF, Sauvageau M, Trayes-Gibson Z, Sanchez-Gomez DB, Morse M, Martin RD, Elcavage LE, Liapis SC, Gonzalez-Celeiro M, et al. Spatiotemporal expression and transcriptional perturbations by long noncoding RNAs in the mouse brain. Proc Natl Acad Sci U S A. 2015; 112:6855–6862. [PubMed: 26034286]

Guan Z, Kuhn JA, Wang X, Colquitt B, Solorzano C, Vaman S, Guan AK, Evans-Reinsch Z, Braz J, Devor M, et al. Injured sensory neuron-derived CSF1 induces microglial proliferation and DAP12-dependent pain. Nat Neurosci. 2016; 19:94–101. [PubMed: 26642091]

Guttman M, Amit I, Garber M, French C, Lin MF, Feldser D, Huarte M, Zuk O, Carey BW, Cassady JP, et al. Chromatin signature reveals over a thousand highly conserved large noncoding RNAs in mammals. Nature. 2009; 458:223–227. [PubMed: 19182780]

Hanz S, Perlson E, Willis D, Zheng J-Q, Massarwa R 'ada, Huerta JJ, Koltzenburg M, Kohler M, van-Minnen J, Twiss JL, et al. Axoplasmic importins enable retrograde injury signaling in lesioned nerve. Neuron. 2003; 40:1095–1104. [PubMed: 14687545]

Hezroni H, Koppstein D, Schwartz MG, Avrutin A, Bartel DP, Ulitsky I. Principles of Long Noncoding RNA Evolution Derived from Direct Comparison of Transcriptomes in 17 Species. Cell Rep. 2015

Hu G, Huang K, Hu Y, Du G, Xue Z, Zhu X, Fan G. Single-cell RNA-seq reveals distinct injury responses in different types of DRG sensory neurons. Sci Rep. 2016; 6:31851. [PubMed: 27558660]

Isoda T, Moore AJ, He Z, Chandra V, Aida M, Denholtz M, Piet van Hamburg J, Fisch KM, Chang AN, Fahl SP, et al. Non-coding Transcription Instructs Chromatin Folding and Compartmentalization to Dictate Enhancer-Promoter Communication and T Cell Fate. Cell. 2017; 171:103–119.e18. [PubMed: 28938112]

Jankowski MP, Cornuet PK, McIlwrath S, Koerber HR, Albers KM. SRY-box containing gene 11 (Sox11) transcription factor is required for neuron survival and neurite growth. Neuroscience. 2006; 143:501–514. [PubMed: 17055661]

Jankowski MP, McIlwrath SL, Jing X, Cornuet PK, Salerno KM, Koerber HR, Albers KM. Sox11 transcription factor modulates peripheral nerve regeneration in adult mice. Brain Res. 2009; 1256:43–54. [PubMed: 19133245]

Jankowski MP, Miller L, Koerber HR. Increased expression of transcription factor SRY-box containing gene 11 (Sox11) enhances neurite growth by regulating neurotrophic factor responsiveness. Neuroscience. 2018

Jing X, Wang T, Huang S, Glorioso JC, Albers KM. The transcription factor Sox11 promotes nerve regeneration through activation of the regeneration-associated gene Sprr1a. Exp Neurol. 2012; T233:221–232.

Kappos EA, Sieber PK, Engels PE, Mariolo AV, D'Arpa S, Schaefer DJ, Kalbermatten DF. Validity and reliability of the CatWalk system as a static and dynamic gait analysis tool for the assessment of functional nerve recovery in small animal models. Brain Behav. 2017; 7:e00723. [PubMed: 28729931]

Kapranov P, Cheng J, Dike S, Nix DA, Duttagupta R, Willingham AT, Stadler PF, Hertel J, Hackermuller J, Hofacker IL, et al. RNA maps reveal new RNA classes and a possible function for pervasive transcription. Science. 2007; 316:1484–1488. [PubMed: 17510325]

Kim D, Langmead B, Salzberg SL. HISAT: a fast spliced aligner with low memory requirements. Nat Methods. 2015; 12:357–360. [PubMed: 25751142]

Kubo T, Yamashita T, Yamaguchi A, Hosokawa K, Tohyama M. Analysis of genes induced in peripheral nerve after axotomy using cDNA microarrays. J Neurochem. 2002; 82:1129–1136. [PubMed: 12358760]

Küry P, Abankwa D, Kruse F, Greiner-Petter R, Müller HW. Gene expression profiling reveals multiple novel intrinsic and extrinsic factors associated with axonal regeneration failure. Eur J Neurosci. 2004; 19:32–42. [PubMed: 14750961]

Li B, Dewey CN. RSEM: accurate transcript quantification from RNA-Seq data with or without a reference genome. BMC Bioinformatics. 2011; 12:323. [PubMed: 21816040]

Lin MF, Jungreis I, Kellis M. PhyloCSF: a comparative genomics method to distinguish protein coding and non-coding regions. Bioinformatics. 2011; 27:i275–i282. [PubMed: 21685081]

Lisi V, Singh B, Giroux M, Guzman E, Painter MW, Cheng Y-C, Huebner E, Coppola G, Costigan M, Woolf CJ, et al. Enhanced Neuronal Regeneration in the CAST/Ei Mouse Strain Is Linked to Expression of Differentiation Markers after Injury. Cell Rep. 2017; 20:1136–1147. [PubMed: 28768198]

Love M, Anders S, Huber W. Differential analysis of count data--the DESeq2 package. Genome Biol. 2014; 15:550. [PubMed: 25516281]

Lyubimova A, Itzkovitz S, Junker JP, Fan ZP, Wu X, van Oudenaarden A. Single-molecule mRNA detection and counting in mammalian tissue. Nat Protoc. 2013; 8:1743–1758. [PubMed: 23949380]

Mahar M, Cavalli V. Intrinsic mechanisms of neuronal axon regeneration. Nat Rev Neurosci. 2018; 19:323–337. [PubMed: 29666508]

Maor-Nof M, Romi E, Sar Shalom H, Ulisse V, Raanan C, Nof A, Leshkowitz D, Lang R, Yaron A. Axonal Degeneration Is Regulated by a Transcriptional Program that Coordinates Expression of Pro- and Anti-degenerative Factors. Neuron. 2016; 92:991–1006. [PubMed: 27889097]

Michaelevski I, Segal-Ruder Y, Rozenbaum M, Medzihradszky KF, Shalem O, Coppola G, Horn-Saban S, Ben-Yaakov K, Dagan SY, Rishal I, et al. Signaling to transcription networks in the neuronal retrograde injury response. Sci Signal. 2010; 3:ra53. [PubMed: 20628157]

Mo A, Mukamel EA, Davis FP, Luo C, Henry GL, Picard S, Urich MA, Nery JR, Sejnowski TJ, Lister R, et al. Epigenomic Signatures of Neuronal Diversity in the Mammalian Brain. Neuron. 2015; 86:1369–1384. [PubMed: 26087164]

Nguyen T, Wong RC-B. Neuroregeneration using in vivo cellular reprogramming. Neural Regeneration Res. 2017; 12:1073–1074.

Ntini E, Louloupi A, Liz J, Muino JM, Marsico A, Ørom UAV. Long ncRNA A-ROD activates its target gene DKK1 at its release from chromatin. Nat Commun. 2018; 9:1636. [PubMed: 29691407]

Patodia S, Raivich G. Role of transcription factors in peripheral nerve regeneration. Front Mol Neurosci. 2012; 5:8. [PubMed: 22363260]

Perlson E, Hanz S, Ben-Yaakov K, Segal-Ruder Y, Seger R, Fainzilber M. Vimentin-dependent spatial translocation of an activated MAP kinase in injured nerve. Neuron. 2005; 45:715–726. [PubMed: 15748847]

Perry RB-T, Ulitsky I. The functions of long noncoding RNAs in development and stem cells. Development. 2016; 143:3882–3894. [PubMed: 27803057]

Perry RB-T, Doron-Mandel E, Iavnilovitch E, Rishal I, Dagan SY, Tsoory M, Coppola G, McDonald MK, Gomes C, Geschwind DH, et al. Subcellular knockout of importin β1 perturbs axonal retrograde signaling. Neuron. 2012; 75:294–305. [PubMed: 22841314]

Pertea M, Pertea GM, Antonescu CM, Chang TC, Mendell JT, Salzberg SL. StringTie enables improved reconstruction of a transcriptome from RNA-seq reads. Nat Biotechnol. 2015; 33:290–295. [PubMed: 25690850]

Preissl S, Fang R, Huang H, Zhao Y, Raviram R, Gorkin DU, Zhang Y, Sos BC, Afzal V, Dickel DE, et al. Single-nucleus analysis of accessible chromatin in developing mouse forebrain reveals cell-type-specific transcriptional regulation. Nat Neurosci. 2018; 21:432–439. [PubMed: 29434377]

Raivich G, Bohatschek M, Da Costa C, Iwata O, Galiano M, Hristova M, Nateri AS, Makwana M, Riera-Sans L, Wolfer DP, et al. The AP-1 transcription factor c-Jun is required for efficient axonal regeneration. Neuron. 2004; 43:57–67. [PubMed: 15233917]

Ravasi T, Suzuki H, Pang KC, Katayama S, Furuno M, Okunishi R, Fukuda S, Ru K, Frith MC, Gongora MM, et al. Experimental validation of the regulated expression of large numbers of non-coding RNAs from the mouse genome. Genome Res. 2006; 16:11–19. [PubMed: 16344565]

Sauvageau M, Goff LA, Lodato S, Bonev B, Groff AF, Gerhardinger C, Sanchez-Gomez DB, Hacisuleyman E, Li E, Spence M, et al. Multiple knockout mouse models reveal lincRNAs are required for life and brain development. Elife. 2013; 2:e01749. [PubMed: 24381249]

Schaukowitch K, Joo J-Y, Liu X, Watts JK, Martinez C, Kim T-K. Enhancer RNA facilitates NELF release from immediate early genes. Mol Cell. 2014; 56:29–42. [PubMed: 25263592]

Seijffers R, Mills CD, Woolf CJ. ATF3 increases the intrinsic growth state of DRG neurons to enhance peripheral nerve regeneration. J Neurosci. 2007; 27:7911–7920. [PubMed: 17652582]

Sharan R, Shamir R. CLICK: a clustering algorithm with applications to gene expression analysis. Proc Int Conf Intell Syst Mol Biol. 2000; 8:307–316. [PubMed: 10977092]

Skene JH, Jacobson RD, Snipes GJ, McGuire CB, Norden JJ, Freeman JA. A protein induced during nerve growth (GAP-43) is a major component of growth-cone membranes. Science. 1986; 233:783–786. [PubMed: 3738509]

Tedeschi A, Dupraz S, Laskowski CJ, Xue J, Ulas T, Beyer M, Schultze JL, Bradke F. The Calcium Channel Subunit Alpha2delta2 Suppresses Axon Regeneration in the Adult CNS. Neuron. 2016; 92:419–434. [PubMed: 27720483]

Tsujino H, Kondo E, Fukuoka T, Dai Y, Tokunaga A, Miki K, Yonenobu K, Ochi T, Noguchi K. Activating transcription factor 3 (ATF3) induction by axotomy in sensory and motoneurons: A novel neuronal marker of nerve injury. Mol Cell Neurosci. 2000; 15:170–182. [PubMed: 10673325]

Ulitsky I. Evolution to the rescue: using comparative genomics to understand long non-coding RNAs. Nat Rev Genet. 2016

Ulitsky I, Maron-Katz A, Shavit S, Sagir D, Linhart C, Elkon R, Tanay A, Sharan R, Shiloh Y, Shamir R. Expander: from expression microarrays to networks and functions. Nat Protoc. 2010; 5:303–322. [PubMed: 20134430]

Ulitsky I, Shkumatava A, Jan CH, Sive H, Bartel DP. Conserved function of lincRNAs in vertebrate embryonic development despite rapid sequence evolution. Cell. 2011; 147:1537–1550. [PubMed: 22196729]

Van der Zee CE, Nielander HB, Vos JP, Lopes da Silva S, Verhaagen J, Oestreicher AB, Schrama LH, Schotman P, Gispen WH. Expression of growth-associated protein B-50 (GAP43) in dorsal root ganglia and sciatic nerve during regenerative sprouting. J Neurosci. 1989; 9:3505–3512. [PubMed: 2552034]

Wang ET, Sandberg R, Luo S, Khrebtukova I, Zhang L, Mayr C, Kingsmore SF, Schroth GP, Burge CB. Alternative isoform regulation in human tissue transcriptomes. Nature. 2008; 456:470–476. [PubMed: 18978772]

Wang F, Flanagan J, Su N, Wang L-C, Bui S, Nielson A, Wu X, Vo H-T, Ma X-J, Luo Y. RNAscope: a novel in situ RNA analysis platform for formalin-fixed, paraffin-embedded tissues. J Mol Diagn. 2012; 14:22–29. [PubMed: 22166544]

Wang L, Park HJ, Dasari S, Wang S, Kocher JP, Li W. CPAT: Coding-Potential Assessment Tool using an alignment-free logistic regression model. Nucleic Acids Res. 2013; 41:e74. [PubMed: 23335781]

Xiang J-F, Yin Q-F, Chen T, Zhang Y, Zhang X-O, Wu Z, Zhang S, Wang H-B, Ge J, Lu X, et al. Human colorectal cancer-specific CCAT1-L lncRNA regulates long-range chromatin interactions at the MYC locus. Cell Res. 2014; 24:513–531. [PubMed: 24662484]

Yao C, Wang J, Zhang H, Zhou S, Qian T, Ding F, Gu X, Yu B. Long non-coding RNA uc.217 regulates neurite outgrowth in dorsal root ganglion neurons following peripheral nerve injury. Eur J Neurosci. 2015; 42:1718–1725. [PubMed: 26032672]

Yasuda M, Tanaka Y, Ryu M, Tsuda S, Nakazawa T. RNA sequence reveals mouse retinal transcriptome changes early after axonal injury. PLoS One. 2014; 9:e93258. [PubMed: 24676137]

Yin K, Deuis JR, Lewis RJ, Vetter I. Transcriptomic and behavioural characterisation of a mouse model of burn pain identify the cholecystokinin 2 receptor as an analgesic target. Mol Pain. 2016; 12

Yu B, Zhou S, Hu W, Qian T, Gao R, Ding G, Ding F, Gu X. Altered long noncoding RNA expressions in dorsal root ganglion after rat sciatic nerve injury. Neurosci Lett. 2013; 534:117–122. [PubMed: 23274483]

Zhang Y, Liu T, Meyer CA, Eeckhoute J, Johnson DS, Bernstein BE, Nusbaum C, Myers RM, Brown M, Li W, et al. Model-based analysis of ChIP-Seq (MACS). Genome Biol. 2008; 9:R137. [PubMed: 18798982]
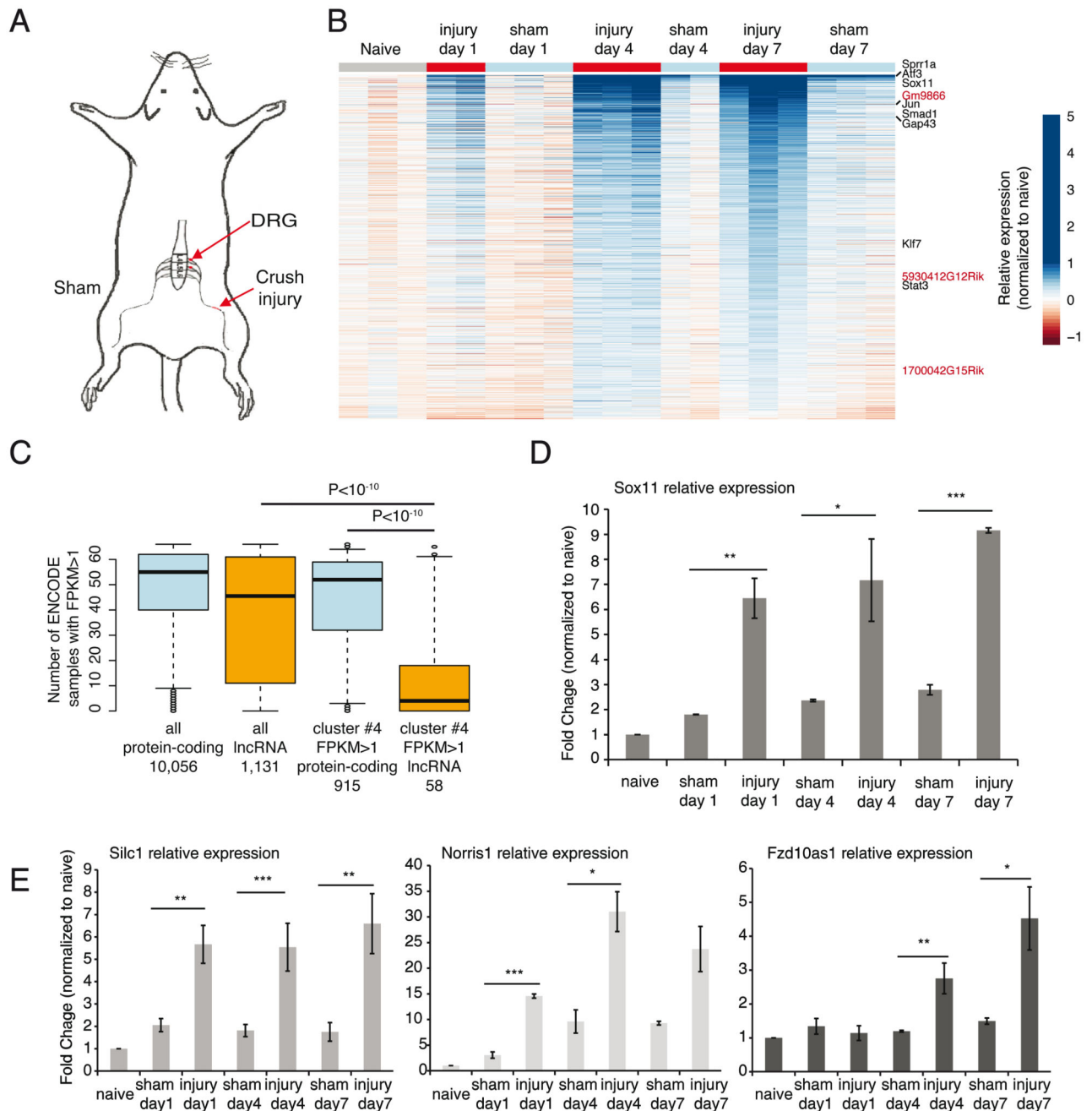
Figure 1. Transcriptional changes in the DRG following sciatic nerve crush.
(**A**) Experimental setup. (**B**) Expression patterns of genes in cluster #4. Each row was normalized to the mean expression pattern in the three replicates of naive DRG. Selected protein-coding (black) and lncRNA (red) genes are indicated. (**C**) Distributions of the number of ENCODE tissue samples in which genes from the indicated groups were expressed. The number of genes in each group appears below the group name. P-values computed using two-sided Wilcoxon test. (**D**) Average expression of *Sox11* in the indicated DRG tissue samples, measured by qRT-PCR, and normalized to β actin. Mean ± SEM, n=3,

* p < 0.05, ** p < 0.005, *** p < 0.001, unpaired two sample t-test. **(E)** Same as D for *Silc1*, N*orris1*, and *Fzd10as1*. See also Figure S1, Data S1, and Data S2.
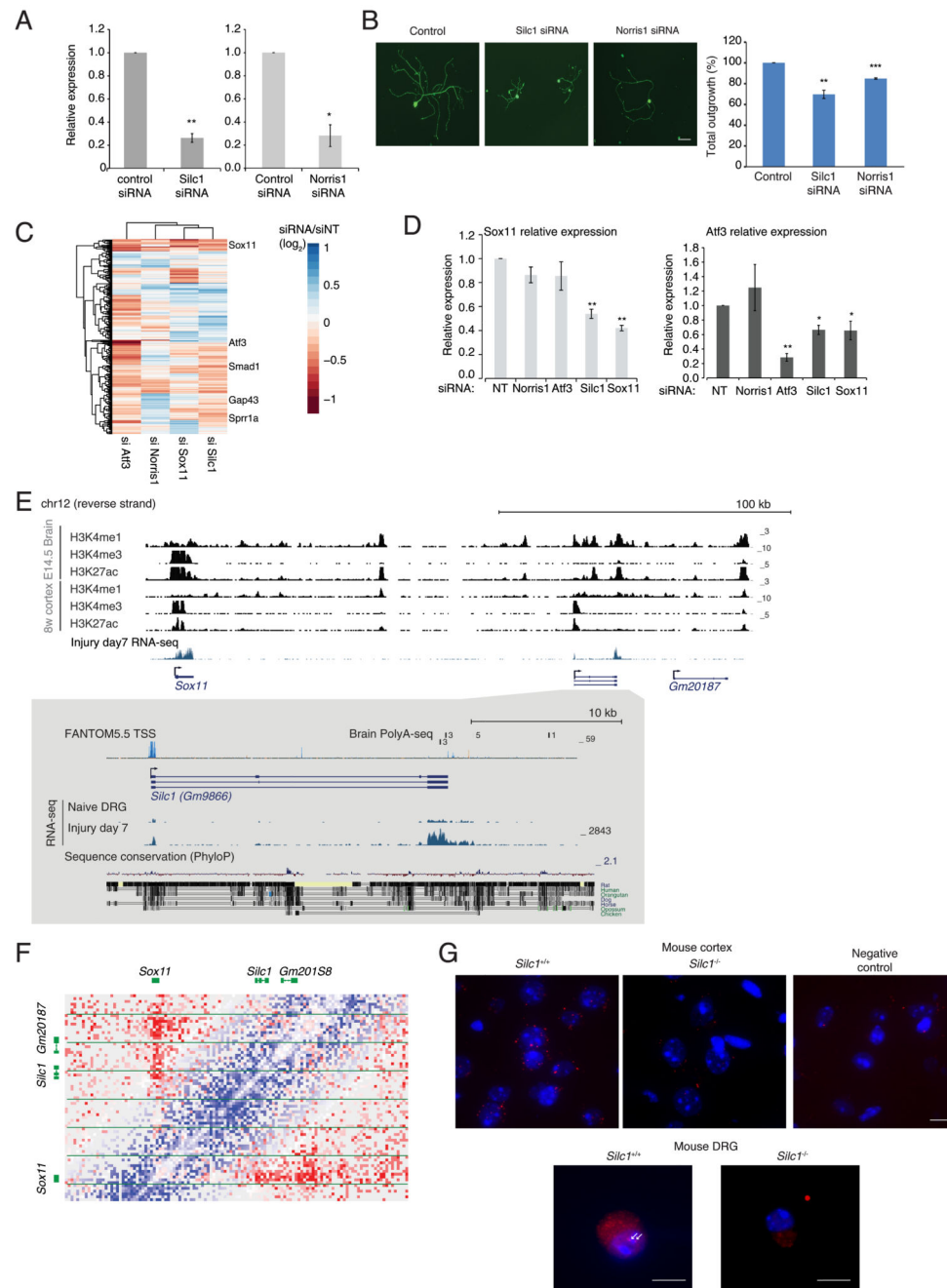
Figure 2. Knockdown of *Silc1* and *Norris1* using RNAi affects neuroregeneration.
(A) qRT-PCR of *Silc1* and *Norris1* following their knockdown in cultured neurons using SMARTpool siRNAs. Mean ± SEM is shown, n=3, * p < 0.05, ** p < 0.005, unpaired two sample t-test. **(B)** Left: representative image of replated neurons following the indicated treatment. Right: quantification of total outgrowth (%) for n>1000 neurons from three biological repeats (Mean ± SEM, n=3, ** p < 0.005, *** p < 0.001, unpaired two sample t-test). Scale bar 80 μm. **(C)** Changes in gene expression following siRNA transfection, normalized to a non-targeting siRNA. Only genes with a log2-transformed absolute change

0.4 are shown. Clustering of rows and columns is based on Euclidean distance. (D) Changes in expression of *Sox11* (top) and *Atf3* (bottom) following the indicated transfections (Mean ± SEM, n=3, * $p < 0.05$, ** $p < 0.005$, unpaired two sample t-test). **(E)** *Silc1* locus outline. ChIP-seq data are from the ENCODE project. Other information from the UCSC genome browser. **(F)** Hi-C data from the mouse brain (Deng et al., 2015) in the *Sox11* downstream region, visualized using JuiceBox (Durand et al., 2016). Red squares correspond to regions with contact frequency higher than background. **(G)** Top: fluorescent *in situ* hybridization (FISH) assay using RNAscope and cortex sections from mice with the indicated genotype. A no-probe control was performed in parallel as an indicator of background staining. Tissues were counterstained with *Silc1* probes (red) and DAPI (blue), and imaged using 150X oil-immersion objective. Scale bar 10 μm. Bottom: smFISH on cultured DRG neurons from *Silc1*$^{+/+}$ and *Silc1*$^{-/-}$ mice using Stellaris probes for *Silc1* (red) and DAPI staining (blue), imaged using 100X oil-immersion objective. Arrows indicate *Silc*1 expression in the cell body nucleus. Scale bar 100 μm. See also Figure S2.
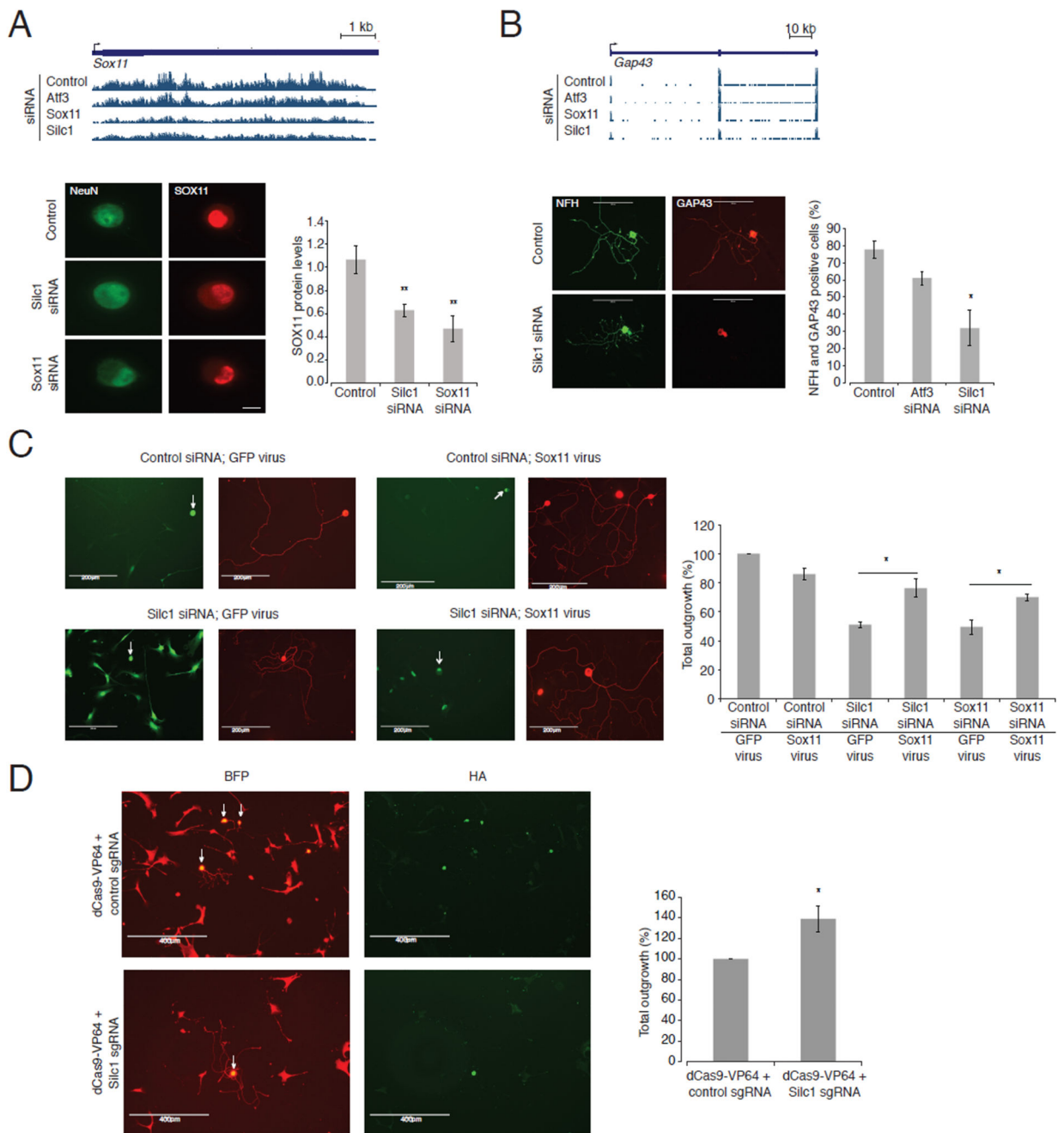
Figure 3. *Silc1* acts through regulation of *Sox11*.
(**A**) Changes in *Sox11* expression in cultured neurons following the indicated condition.
Top: Normalized RNA-seq coverage; Left: staining for NeuN and SOX11 proteins; Right:
Quantification of n=60 cells (Mean ± SEM, ** p < 0.005, unpaired two sample t-test). Scale
bar 40 μm. (**B**) Changes in *Gap43* expression following the indicated KD. Top: Normalized
RNA-seq coverage; Left: staining with anti-NFH for process length determination and with
anti-GAP43. Scale bars 200 μm; Right: Quantification of NFH and GAP43 positive cells in
n>1000 cells, 3 biological repeats (Mean ± SEM, * p < 0.05, unpaired two sample t-test).

(C) Neurite outgrowth following combined treatment of cultured DRG with siRNAs and lentiviruses. The cells were stained with anti-NFH and only GFP positive cells were imaged for process length determination. Scale bars 200 μm. Right: quantification of n=40 cells. 3 biological repeats (Mean ± SEM, * $p < 0.05$, unpaired two sample t-test). **(D)** Activation of *Silc1* using CRISPRa in cultured DRG increases neurite outgrowth. Only cells that were positive for NFH, HA, and BFP were imaged for process length determination. Scale bars 400 μm. Right: quantification of n>700 cells, 3 biological repeats (Mean ± SEM, * $p < 0.05$, unpaired two sample t-test). See also Figure S3.
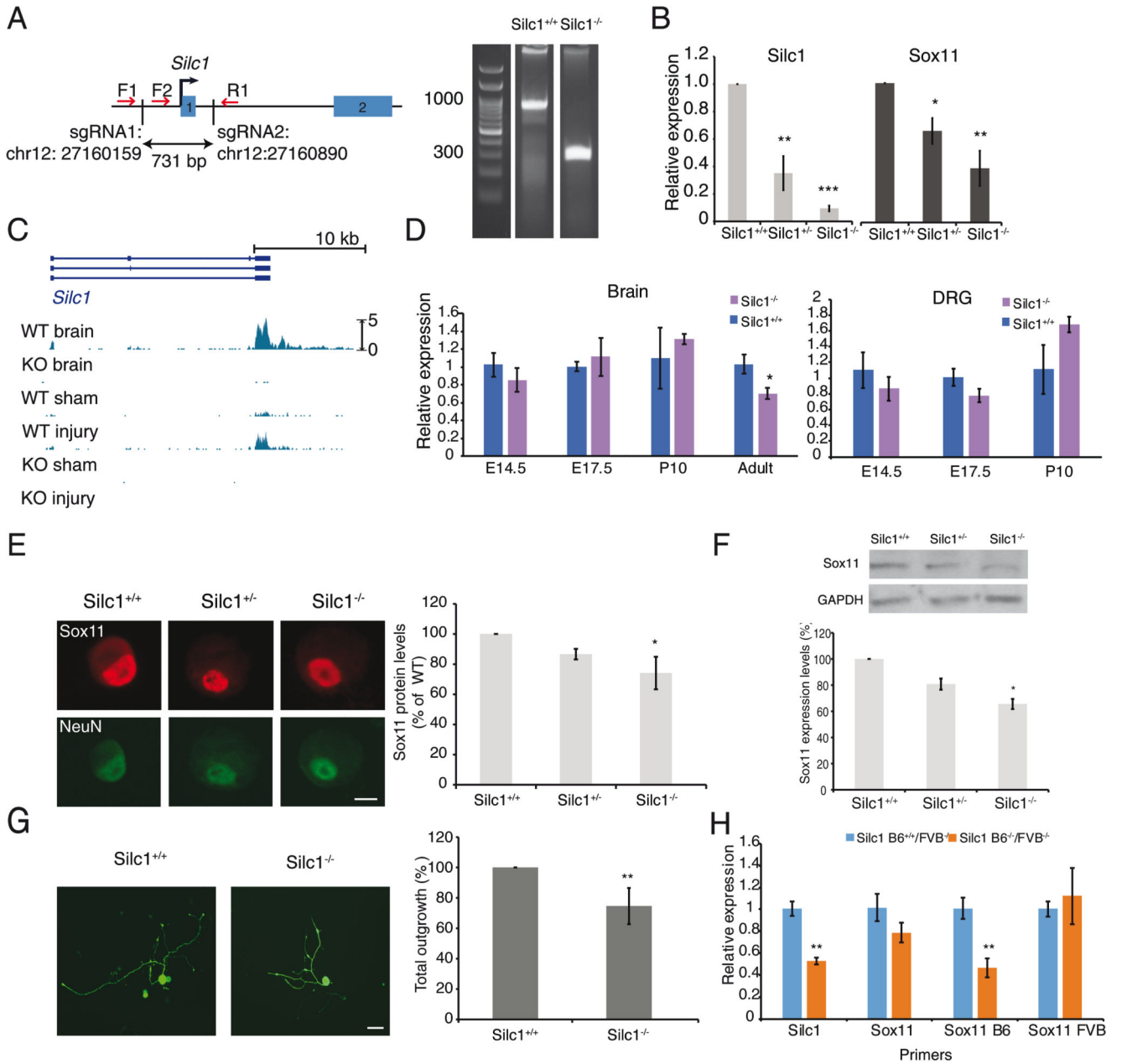
Figure 4. Reduced regeneration in cultured *Silc1*^{-/-} DRG.
(A) Left: *Silc1* KO using CRISPR/Cas9. Right: RT-PCR confirmation using F1 and R1 primers (see Methods). (B) Expression of *Silc1* and *Sox11* in cultured DRG neurons 24 hours after re-plating. n=3, Mean ± SEM is shown, * p < 0.05, ** p < 0.005, and *** p < 0.001, unpaired two sample t-test. (C) RNA-seq read coverage in the *Silc1* locus in the brain and DRG of WT and *Silc1*^{-/-} mice. Representative samples are shown, normalized together to the same scale. (D) Expression of *Sox11* mRNA measured using qRT-PCR with brain and DRG tissue from the indicated stage. n=3-7, Mean ± SEM is shown, * p < 0.05, unpaired two sample t-test. (E) Left: Staining with anti-SOX11 and anti-NeuN in representative DRG culture cells. Right: Quantification of staining in 70-80 cells. Scale bar 20 μm. (F) Western

blot using SOX11 and GAPDH antibodies and whole brain tissue from mice with the indicated genotype. n=3, Mean ± SEM is shown, * $p < 0.05$, unpaired two sample t-test. **(G)** Total neurite outgrowth in cultured DRG 24 hours following replating. Left: quantification of n>1000 cells. 3 biological repeats, Mean ± SEM is shown, ** $p < 0.005$, unpaired two sample t-test. Right: representative cells stained with anti-NFH. Scale bar 80 μm. **(H)** Expression of Silc1 and Sox11 mRNA measured with qRT-PCR on cDNA from progeny of C57BL/6J (B6) Silc1$^{+/-}$ and FVB/NJ Silc1$^{+/+}$ mice. n=3, Mean ± SEM, * $p < 0.05$, unpaired two sample t-test. See also Figure S4.
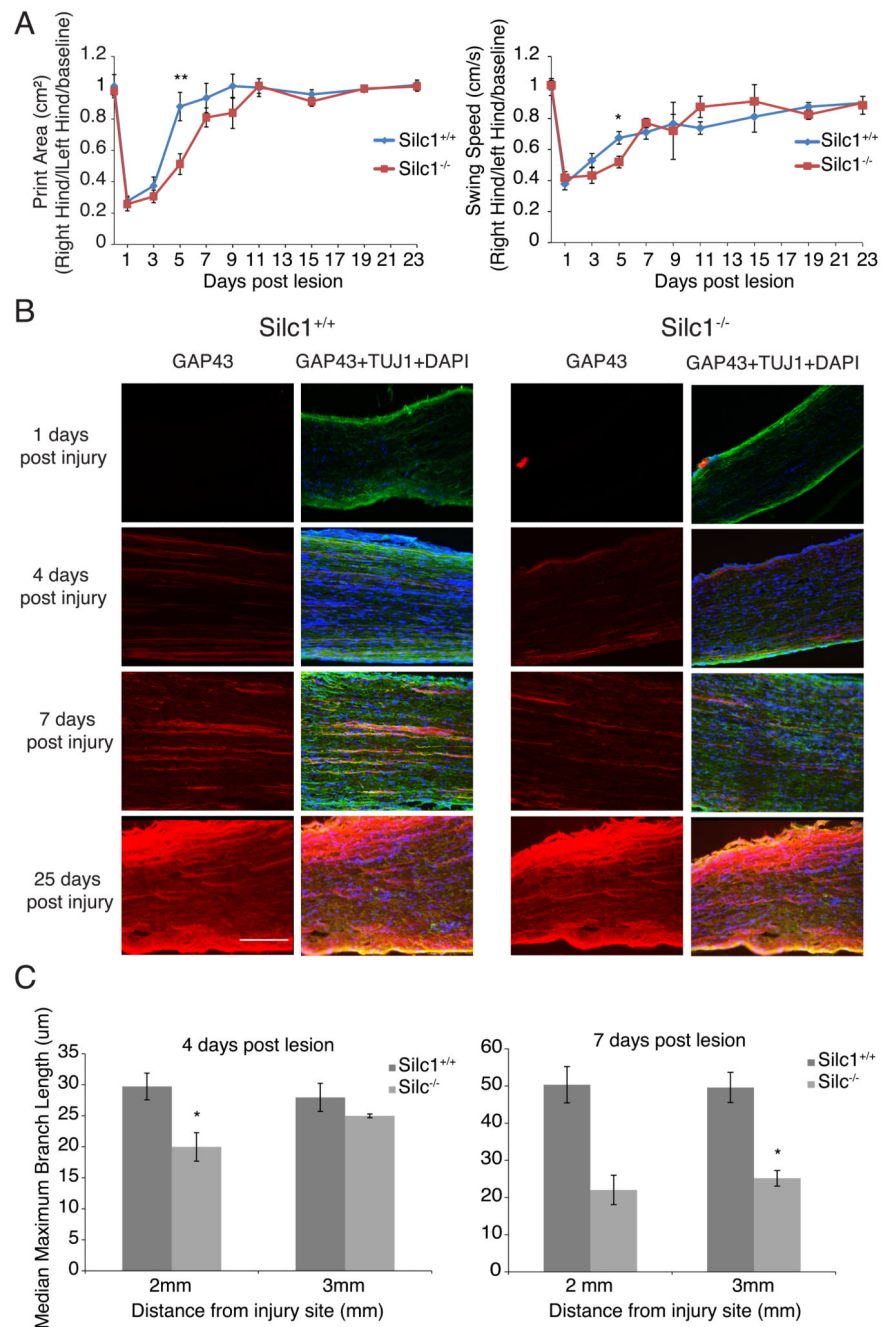
Figure 5. Delayed regeneration in *Silc1*^{-/-} mice.
(**A**) Left: The print area of the ipsilateral hind paw is expressed in relation to that of the contralateral hind paw and to the baseline of each animal over subsequent days (cm^2). ** p<0.005 using two-way ANOVA. Data are expressed as average ± SEM (WT n=14; *Silc1*^{-/-} n=13). Right: The swing speed of the ipsilateral hind paw is expressed in relation to that of the contralateral hind paw and to the baseline of each animal over subsequent days (cm/s). Asterisk indicates * p<0.05 using two-way ANOVA. Data are expressed as average ± SEM (WT n=14 and *Silc1*^{-/-} n=13). (**B**) Representative images of longitudinal sections 2 mm

proximal to the injury site, from WT and *Silc1*^{-/-} sciatic nerve, 1, 4, 7, and 25 days after sciatic lesion. Staining for GAP43 (red), TUJ1 (green), and DAPI (blue). 20x magnification using Leica DM4000 B fluorescence microscopy. Scale bar 100 μm. **(C)** Quantification of axonal fibers branch length (um), 2mm and 3mm proximal to injury site. Median ± SEM, n=3, asterisk denotes $p < 0.05$ (independent two-sample t-test). The Quantification was done using script in Fiji software (see Methods). See also Figure S5.
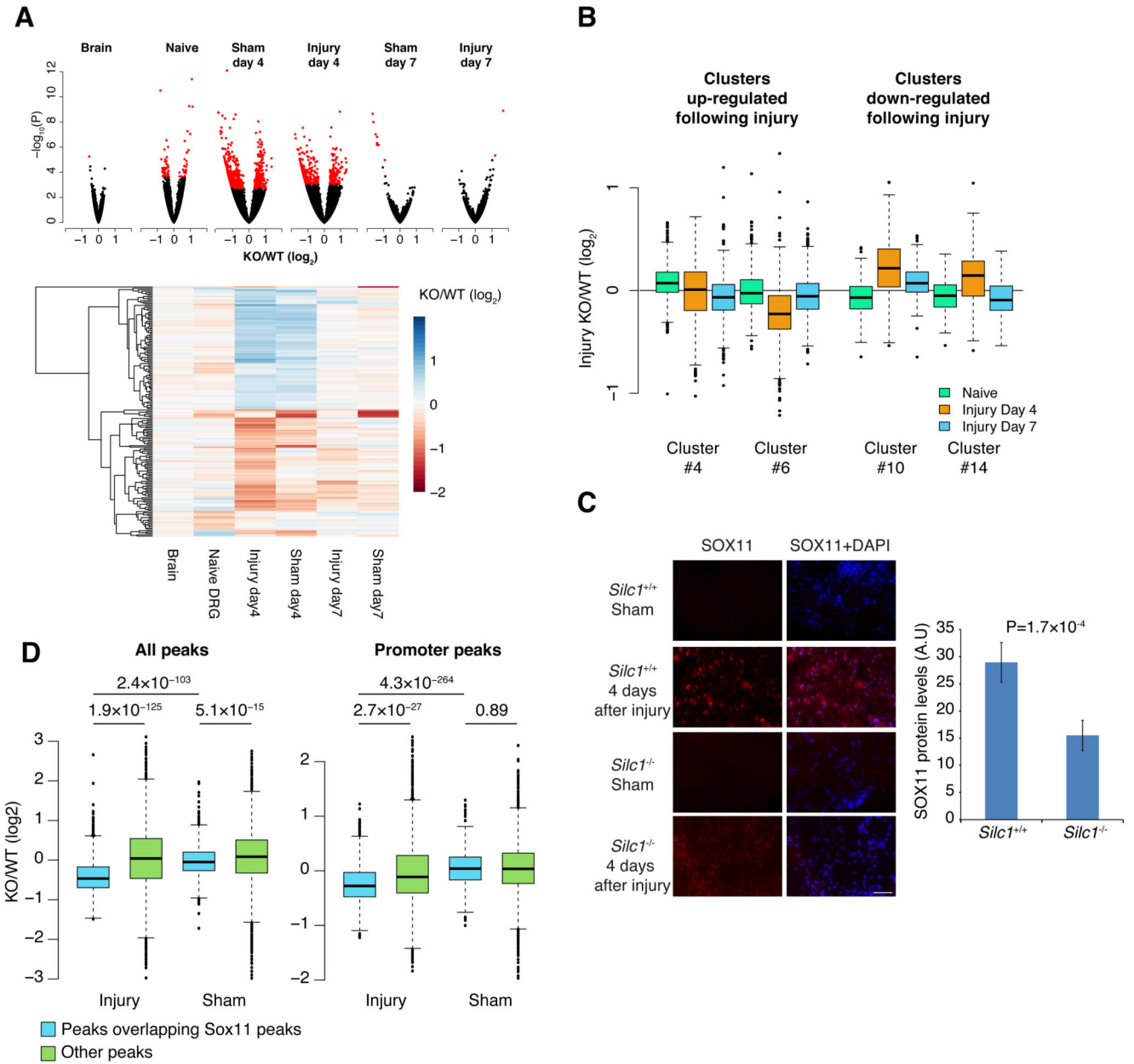
Figure 6. Changes in gene expression and chromatin accessibility in *Silc1*-/- mice.
(A) Top: Volcano plots showing changes in gene expression in *Silc1*-/- mice compared to WT littermates. Red points correspond to adjusted P-value < 0.05. Bottom: Heatmap of the same fold changes, omitting genes in clusters #2, 5, 7, and 8, which like represent genes expressed in non-neuronal cells (Figure S1A). **(B)** Changes in gene expression in the injured DRG of genes in indicated clusters of response to injury (Figure S1A), at the indicated day following injury. **(C)** Differences in chromatin accessibility in peaks identified in ATAC-seq data (see Methods), at four days following injury or sham operation, for peaks overlapping regions bound by Sox11 in neurons (Bergsland et al., 2011) and the other regions. **(D)** Staining of SOX11 in the DRG at day 4 following sham operation or sciatic nerve crush.

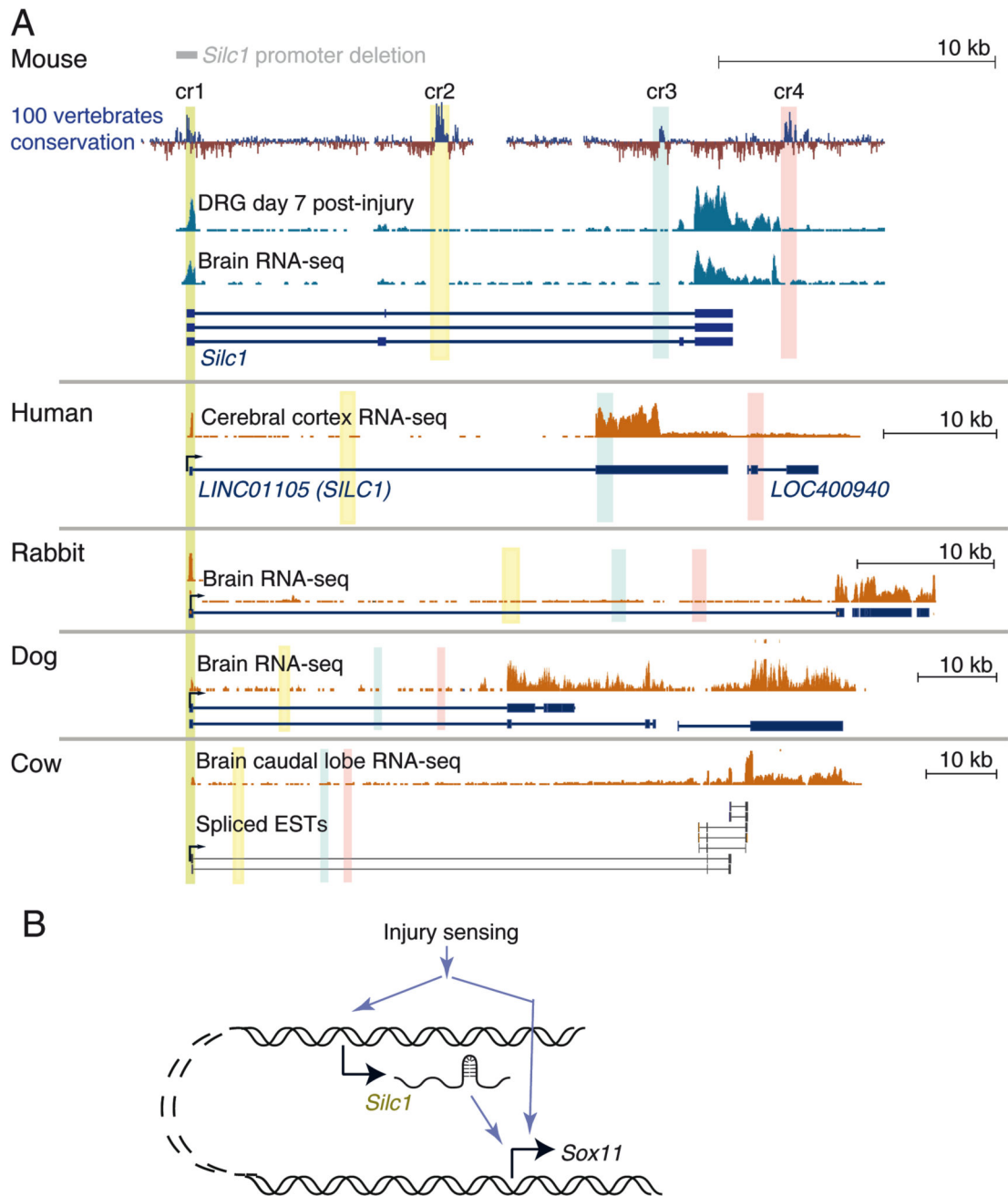Scale bar 100 μm. n=3, Mean ± SEM is shown, unpaired two sample t-test. See also Figure S6 and Data S3.

Figure 7. Conservation of *Silc1* lncRNA in mammals.
(**A**) The *Silc1* locus in five mammalian species. Shaded regions indicate four regions of high sequence conservation. Gene models in human and mouse are from RefSeq, and in rabbit and dog from PLAR transcript reconstructions (Hezroni et al., 2015). RNA-seq datasets from brain regions were taken from publically-available datasets: SRP100399 (mouse), SRP042639 (cow), SRP009687 (dog), SRP009665 (rabbit), and HPA (Fagerberg et al., 2014) (human). (**B**) Model for Silc1 activity. See also Figure S7.